

Volumetric Neuroimaging of the Atlantic White-Sided Dolphin (*Lagenorhynchus acutus*) Brain From In Situ Magnetic Resonance Images

ERIC W. MONTIE,^{1*} GERALD SCHNEIDER,² DARLENE R. KETTEN,¹
LORI MARINO,³ KATIE E. TOUHEY,⁴ AND MARK E. HAHN^{1*}

¹Department of Biology, Woods Hole Oceanographic Institution,
Woods Hole, Massachusetts

²Department of Brain and Cognitive Sciences, MIT, Cambridge, Massachusetts

³Neuroscience and Behavioral Biology Program, Emory University, Atlanta, Georgia

⁴Cape Cod Stranding Network, Buzzards Bay, Massachusetts

ABSTRACT

The structure and development of the brain are extremely difficult to study in free-ranging marine mammals. Here, we report measurements of total white matter (WM), total gray matter (GM), cerebellum (WM and GM), hippocampus, and corpus callosum made from magnetic resonance (MR) images of fresh, postmortem brains of the Atlantic white-sided dolphin (*Lagenorhynchus acutus*) imaged in situ (i.e., the brain intact within the skull, with the head still attached to the body). WM:GM volume ratios of the entire brain increased from fetus to adult, illustrating the increase in myelination during ontogeny. The cerebellum (WM and GM combined) of subadult and adult dolphins ranged from 13.8 to 15.0% of total brain size, much larger than that of primates. The corpus callosum mid-sagittal area to brain mass ratios (CCA/BM) ranged from 0.088 to 0.137, smaller than in most mammals. Dolphin hippocampal volumes were smaller than those of carnivores, ungulates, and humans, consistent with previous qualitative results assessed from histological studies of the bottlenose dolphin brain. These quantitative measurements of white matter, gray matter, corpus callosum, and hippocampus are the first to be determined from MR images for any cetacean species. We establish here an approach for accurately determining the size of brain structures from in situ MR images of stranded, dead dolphins. This approach can be used not only for comparative and developmental studies of marine mammal brains but also for investigation of the potential impacts of natural and anthropogenic chemicals on neurodevelopment and neuroanatomy in exposed marine mammal populations. Anat Rec, 291:263–282, 2008. © 2008 Wiley-Liss, Inc.

Key words: cetacean; dolphin; MRI; white matter; cerebellum; corpus callosum; hippocampus; brain

Grant sponsor: Environmental Protection Agency; Grant number: U-91616101-2; Grant sponsor: the National Woman's Farm and Garden Association; Grant sponsor: the Quebec Labrador Fund/Atlantic Center for the Environment; Grant sponsor: Woods Hole Oceanographic Institution; Grant sponsor: the Sawyer Endowment; Grant sponsor: Walter A. and Hope Noyes Smith.

Dr. Montie's present address is College of Marine Science, University of South Florida, 140 Seventh Avenue, South, St. Petersburg, FL 33701-5016.

*Correspondence to: Mark E. Hahn, Department of Biology, WHOI, MS#32, Woods Hole, MA 02543. Fax: 508-457-2134.

E-mail: mhahn@whoi.edu or Eric W. Montie, College of Marine Science, University of South Florida, 140 Seventh Avenue, South, St. Petersburg, FL 33701-5016. Fax: 727-553-1193. E-mail: emontie@marine.usf.edu

Received 17 October 2007; Accepted 3 December 2007

DOI 10.1002/ar.20654

Published online in Wiley InterScience (www.interscience.wiley.com).

Odontocetes (toothed whales, dolphins, and porpoises) have undergone unique anatomical adaptations to an aquatic environment. One significant modification is in brain size. Several odontocete species have encephalization quotients (a measure of relative brain size) that are second only to modern humans (Ridgway and Brownson, 1984; Marino, 1998). Several studies of odontocete neuroanatomy have been completed, as reviewed by Morgane et al. (1986) and Ridgway (1990). However, few studies have focused on quantitative measurements of odontocete brain structures (Tarpley and Ridgway, 1994; Marino et al., 2000). Fewer studies have focused on odontocete prenatal neuroanatomy or provided quantitative data on prenatal brain structures (Marino et al., 2001a).

Magnetic resonance imaging (MRI) has recently been used to study the neuroanatomy of the Atlantic white-sided dolphin (*Lagenorhynchus acutus*), the beluga whale (*Delphinapterus leucas*), the fetal common dolphin (*Delphinus delphis*), the bottlenose dolphin (*Tursiops truncatus*), the harbor porpoise (*Phocoena phocoena*), the dwarf sperm whale (*Kogia simus*), the spinner dolphin (*Stenella longirostris orientalis*), and the killer whale (*Orcinus orca*; Marino et al., 2001a–c, 2003a,b, 2004a,b; Montie et al., 2007). MRI offers a nondestructive method of acquiring a permanent archive of external and internal brain structure data. MRI coupled with advanced software image analysis can accurately determine regional brain volumes, while traditional dissection and photography may introduce error in performing quantitative measurements.

Quantitative measurements of the size of brain structures can be used not only to study comparative anatomy and development of cetacean brains but also to investigate emerging threats to marine mammals. These include anthropogenic chemicals such as hydroxylated polychlorinated biphenyls (OH-PCBs; Sandala et al., 2004; Houde et al., 2006; McKinney et al., 2006) and polybrominated diphenyl ethers (PBDEs; De Boer et al., 1998), as well as biotoxins from harmful algal blooms (Scholin et al., 2000). These chemicals can target the brain (Viberg et al., 2003; Kimura-Kuroda et al., 2005; Silvagni et al., 2005). For example, domoic acid (a type of biotoxin produced by some diatom *Pseudo-nitzschia* species and associated with harmful algal blooms) is neurotoxic and has been shown to cause bilateral hippocampal atrophy in California sea lions (Silvagni et al., 2005). It is possible that biotoxins and environmental pollutants cause subtle differences in the size of brain structures that are not detectable to the unaided eye; therefore, volumetric neuroimaging would be a valuable approach to identify subtle abnormalities. However, there is a lack of information about normative size ranges and developmental patterns for cetacean brain structures that may be sensitive to these etiologic agents.

Previously, we presented the first anatomically labeled MRI-based atlas of the subadult and fetal brain of the Atlantic white-sided dolphin from in situ MR images of fresh, postmortem brains intact, within the skull, with the head still attached to the body (Montie et al., 2007). Our goal in the present study was to establish a quantitative approach to determine the size of brain structures from in situ MR images of the Atlantic white-sided dolphin. Specifically, the objectives of this study were to (a)

validate our techniques by determining if MRI coupled with advanced software image processing and segmentation could accurately determine volumes, (b) determine the white matter and gray matter volumes of the total brain and cerebellum along an ontogenetic series using MR images, and (c) from MR images, determine the mid-sagittal area of the corpus callosum and the volumes of the left and right hippocampal formation.

MATERIALS AND METHODS

Specimens

The Atlantic white-sided dolphin specimens used in this study stranded live on the beaches of Cape Cod, Massachusetts, between 2004 and 2005 (Table 1). Stranded animals were usually first reported by the public and then responded to by the Cape Cod Stranding Network (CCSN) in Buzzards Bay, MA. The specimens were either found freshly dead or were humanely euthanized by stranding response personnel or by local veterinarians because of poor health. Less than 24 hr had passed since the time of death in all cases. Euthanasia of these animals was approved by the National Marine Fisheries Service (NMFS) Marine Mammal Health and Stranding Response Program (MMHSRP). The use of these specimens for MRI scanning and brain studies was approved by the Institution Animal Care and Use Committee (IACUC) at the Woods Hole Oceanographic Institution (WHOI).

Upon death or retrieval, the specimens were immediately transported to the WHOI necropsy facility where total body weights and morphometric measurements were recorded. Specimens were then prepared for MRI. The headcoil of the MRI scanners had a circumference of 80 cm. Therefore, the blubber, nuchal fat, and semispinalis muscle of specimens that had an axillary girth greater than 80 cm were removed from the head region. The pectoral and dorsal fins were removed from all carcasses. The specimens were then washed, dried, and placed in transport bags with ice surrounding the head. The specimens were then immediately transported to the MRI facility or temporarily stored at 4°C until imaging could be completed. The time of the MRI was recorded. After imaging, the specimen was transported back to WHOI and stored at 4°C overnight. A complete necropsy was performed the next day. The brain was removed, weighed, and archived whole in 10% neutral buffered formalin or at –80°C.

The specimens were classified as fetuses, neonates (126 cm to 140 cm), subadults (defined as reproductively immature, i.e., females of body length from 141 to 201 cm, and males of body length from 141 to 210 cm), or adults. Total length measurements were used in this classification, consistent with those previously determined by Sergeant et al. (1980). In addition, reproductive state (lactation and pregnancy indicated sexual maturity for females) and measurement of gonads (weight and macroscopic examination) also helped in classification of the specimens into the appropriate age class. Teeth were archived for future aging of dolphins.

Magnetic Resonance Data Acquisition

MR images of the brain in situ were acquired in coronal and sagittal planes with either a 1.5 T Siemens

TABLE 1. Stranding and life history information of Atlantic white-sided dolphin specimens in which magnetic resonance imaging (MRI) was performed

Field ID	Date/time of death	Location	Hours to MRI	Condition Code ¹	Stranding type	Sex	Length (cm)	Age Class	Weight (kg)	Brain Lesion ²
CCSN04-195-La	Sept 14, 2004 at 17:36	Herring River Gut, Wellfleet, MA	3	1	single	m	192	subadult	73.5	no
CCSN05-037-La	Feb15, 2005 at 14:30	Chipman's Cove, Wellfleet, MA	10	1	mass	f	206	adult	125	no
CCSN05-038-La ³	February 15, 2005	Chesquesset Neck, Wellfleet, MA	<24	2	mass	f	208	lactating adult	125	yes
CCSN05-039-La	February 15, 2005	Chesquesset Neck, Wellfleet, MA	<24	2	mass	f	211	pregnant adult	146	no
CCSN05-039-Fetus-La	February 15, 2005	Chesquesset Neck, Wellfleet, MA	<24	2	mass	m	44	fetus	1.394	no
CCSN05-040-La	February 15, 2005	Chesquesset Neck, Wellfleet, MA	<24	2	mass	f	204	pregnant adult	123.6	no
CCSN05-040-Fetus-La	February 15, 2005	Chesquesset Neck, Wellfleet, MA	<24	2	mass	m	54	fetus	2.431	no
CCSN05-084-La	March 19, 2005 at 14:15	Wellfleet, MA	5	1	single	m	156	subadult	42.56	no
CCSN05-231-La	Sept 26, 2005 at 13:30	Sandy Neck, Barnstable, MA	10	1	single	f	137	neonate	30	no
CCSN05-232-La ³	Oct 4, 2005 at 12:22	Nauset Beach, Eastham, MA	11	1	single	f	185.5	subadult	77.5	yes

¹A condition code of 1 indicates that the dolphin was euthanized, while a condition code of 2 indicates that the dolphin was found dead but the specimen was in fresh condition (i.e., less than 24 hours had passed since the time of death).

²Brain pathologies were found using MR images.

³Segmentation was not completed on these specimens because of gross brain pathologies.

Vision scanner (Siemens, Munich, Germany) at the Massachusetts Eye and Ear Infirmary (MEEI), Massachusetts General Hospital, Boston, MA, or a 1.5 T Siemens Symphony scanner (Siemens, Munich, Germany) at Shields MRI and Computed Tomography (CT) of Cape Cod, Hyannis, MA. Two-dimensional proton density (PD) and T2-weighted images were acquired using a fast spin-echo sequence with the following parameters: TE = 15/106 msec for PD and T2, respectively; TR = 9,000 msec; slice thickness = 2 mm; flip angle = 180°; FOV = 240 × 240 mm; matrix = 256 × 256; voxel size = 0.9 × 0.9 × 2.0 mm. For fetal brains, the parameters were altered because of the small size of the brain: TE = 15/106 msec for PD and T2, respectively; TR = 8,000 msec; slice thickness = 2 mm; flip angle = 180°; FOV = 200 × 200 mm; matrix = 256 × 256; voxel size = 0.8 × 0.8 × 2.0 mm.

Image Processing

Visualization was completed first on the MRI unit. Postprocessing, segmentation (i.e., assigning pixels to particular structures), volume analysis, and three-dimensional (3D) reconstructions of MR images were performed using the software program AMIRA 3.1.1 (Mercury Computer Systems, San Diego, CA). Segmentation and volume analysis were not completed on specimens that contained gross brain pathologies, as discovered by MRI (Table 1). Native (i.e., no processing of MRI data) T2- and PD-weighted images from each specimen were examined in AMIRA, and the quality of images was evaluated. The data were then processed to ensure adequate threshold segmentation of the brain and cerebellum into white matter (WM) and gray matter (GM) using methods similar to those described by Evans et al. (2006). Threshold segmentation is an automated technique that allows the software user to select pixels with signal intensity values within a defined range.

The image processing consisted of the following steps. First, original T2- and PD-weighted DICOM images were corrected for image intensity nonuniformity by applying a Gaussian filter. The processed results were then subtracted from the original images to generate a "filtered" image set. The new image set was rotated and realigned around the *y*-axis to correct for head tilt and/or differences in head position. From this "filtered and realigned" data set, a brain surface mask was produced to determine edges for digital removal of nearby blubber, muscle, skull, and other head anatomy. The mask was constructed by manually tracing the surface of the brain and deleting all pixels outside this trace for each MR image. These resulting images are referred to as the "processed" PD and T2 images (vs. the original "native" PD and T2 images).

Rilling and Insel (1999) describe the theory of why image processing is necessary for accurate threshold segmentation. An MR image is a map of pixels that are described by different signal intensities. In PD- and T2-weighted images, pixel signal intensity values are lower for WM and higher for GM. AMIRA software can be instructed to select pixels with signal intensity values of a defined range. Thus, in principle, it should be easy to separate WM and GM of native PD- and T2-weighted images using computerized thresholding. However, most MRI scans contain gradients of signal intensity values,

which cause WM and GM in one part of the image to have different signal intensities than those in another region. Hence, a single threshold range cannot capture the WM and GM for an entire slice. This problem is remedied by the application of a Gaussian filter to the native images (i.e., where each pixel is defined by a signal intensity value) to generate filtered results (i.e., a new set of signal intensity values) followed by subtraction of these filtered results from the native images to produce the "processed" images (i.e., where each pixel of the image set is now defined by a new signal intensity value). This processing corrects for the uneven illumination of the scene that is inherent in MR images.

However, a drawback of image processing is a loss of resolution, as observed by Evans et al. (2006). Because of this, we chose to manually segment structures such as the corpus callosum and hippocampus from native images (see Materials and Methods section, Segmentation Analysis). In addition, it was not necessary to correct for signal intensity nonuniformity because manual tracing of structures does not depend on threshold segmentation.

Volume Validation Experiments

Comparisons of expected and segmented volumes of water. Processing of MR images was required for threshold segmentation of brains into WM and GM, as described previously. Therefore, it was important to determine whether our segmentation technique using processed images was accurate. In this experiment, MR imaging was completed on three separate cylindrical vials containing a weighed amount of water (19.8 ± 0.2 ml or the expected volume). Water was used because of the high signal intensity observed in PD- and T2-weighted images. Even though water in brain tissue occurs in varying concentrations and geometries, cylindrical vials of pure water served as a useful surrogate in these volume validation experiments, given the practical limitations of the experiments. Two-dimensional PD- and T2-weighted images of the cylindrical vials were acquired using a fast spin-echo sequence with parameters similar to those used for specimen scanning: TE = 15/106 msec for PD and T2, respectively; TR = 2,500 msec; slice thickness = 2 mm; flip angle = 180°; FOV = 240 × 240 mm; matrix = 256 × 256; voxel size = 0.9 × 0.9 × 2.0 mm. Native T2- and PD-weighted images from each vial were loaded into AMIRA, and the quality of images was evaluated. The image processing of the T2 and PD native images of the vials followed steps similar to those taken in processing the images of the specimen brains, including the correction for image intensity nonuniformity and realignment. Three different processing conditions were applied to native PD and T2 images: (1) application of a Gauss filter three successive times with sigma = 10 and kernel = 21 followed by subtraction of these results; (2) application of a Gauss filter sixteen successive times with sigma = 10 and kernel = 21 followed by subtraction of these results; (3) application of a Gauss filter three successive times with sigma = 10 and kernel = 21 followed by subtraction of these results and then realignment, which consisted of rotating the images 3 degrees around the *y*-axis. These sigma and kernel values were chosen because these values were used in the processing of native PD and T2

specimen images. Rotation of 3 degrees around the global y -axis was evaluated as the realignment parameter because this rotation was often applied to specimen images to remove head tilt. The volumes of water for these different image-processing conditions were then determined using techniques identical to those used in specimen segmentation (i.e., specifying a defined range of signal intensities for water followed by manual editing). Three measurement replicates were completed. The segmented volumes were compared with the expected volumes and root mean squared errors (RMSE) and percent errors (% error) were calculated for each condition.

Comparisons of expected and segmented volumes of brain tissue. We also performed an experiment with actual brain tissue to determine whether the image processing and segmentation procedure in this study was accurate. In this experiment, MR imaging was completed on two dissected regions of the cerebellum from a formalin-fixed brain (CCSN05-038-La). These regions were comprised of WM and GM. Two-dimensional PD- and T2-weighted images were acquired using a fast spin-echo sequence with parameters similar to those used for specimen scanning: TE = 15/106 msec for PD and T2, respectively; TR = 4,060 msec; slice thickness = 2 mm; flip angle = 180°; FOV = 240 × 240 mm; matrix = 256 × 256; voxel size = 0.9 × 0.9 × 2.0 mm. After MRI, the total volumes displaced by the cerebellum samples (i.e., expected total slice volume) were measured separately. The WM and GM were then dissected and separated, and the volumes displaced by each tissue type (i.e., expected WM and GM volumes) were also measured. Native PD- and T2-weighted images from each cerebellum sample were loaded into AMIRA, and the quality of images was evaluated. The image processing of the PD and T2 native images of the vials followed steps similar to those taken in processing the images of the specimen brains, including the correction for image intensity nonuniformity and realignment. A Gauss filter (sigma = 10; kernel = 21) was applied to the PD native images 10 successive times. The filter results were then subtracted from the native PD images to acquire a new image set. These images were then rotated 2 degrees around the y -axis. The volumes of WM and GM of the native and processed PD image set were then determined using techniques identical to those used in specimen segmentation. Three measurement replicates were completed. The segmented volumes were compared with the expected volumes and RMSEs and % errors were calculated for each condition.

Comparisons of manual and threshold segmentation volumes. We performed an experiment that compared threshold segmentation-derived volumes (of WM and GM) of both native and processed PD images (with the application and subtraction of a Gauss filter but not realignment) to manual segmentation volumes (of WM and GM) derived from manually tracing the boundaries of WM and GM. We did not compare cerebrospinal fluid (CSF) volumes because the volume measurements of CSF are most likely inaccurate due to postmortem leakage. This experiment was completed on three coronal PD-weighted brain sections from separate specimens (CCSN05-040-La, CCSN05-037-La, and CCSN05-231-La) at the level of the inferior and superior

colliculi. The Gauss filter processing of the PD images in this experiment followed the same steps as those taken in the processing of the specimen brains. The volumes of WM and GM of the native and processed PD images were then determined using techniques identical to those used in specimen threshold segmentation. Three measurement replicates were completed. The threshold volumes were compared with the manual volumes and RMSEs and % errors were calculated for each condition.

Anatomic Labeling and Nomenclature

Previously, we presented the first anatomically labeled MRI-based atlas of the subadult and fetal brain of the Atlantic white-sided dolphin (Montie et al., 2007). Anatomical structures were identified and labeled in coronal and sagittal MR images of these brains. The volumetric measurements of brain structures for the fetus (CCN05-040-La-fetus) and the subadult (CCSN05-084-La) examined in that study are presented in the present study. In both studies, the anatomical nomenclature was adopted from Morgane et al. (1980).

Segmentation Analysis

For specimens in which the MRIs were of high quality, the size of brain structures were determined using image segmentation. Measurements of brain structures included the following: total brain volume from “processed” PD-weighted images; total brain tissue (GM and WM) volumes from “processed” T2-weighted images (for fetus segmentation) or “processed” PD-weighted images (for the neonate, subadult, and adult segmentation); cerebellum tissue (GM and WM) volumes by manual segmentation of the previously generated total brain tissue label map (using a visual representation of the segmentation); corpus callosum mid-sagittal area from native and processed PD-weighted sagittal images; and hippocampus volumes from native T2-weighted images. These measurements are described in more detail below.

Total brain. Total brain segmented volumes were calculated by integrating the area of the selected tissue for each slice of the brain surface mask. The caudal boundary of the brain was defined by the posterior aspect of the foramen magnum. Virtual brain weight was calculated by multiplying the total brain segmented volume by the assumed specific gravity of brain tissue, 1.036 g/cm³ (Stephan et al., 1981).

Total brain WM and GM volumes were determined by threshold segmentation of the brain surface mask followed by manual editing of each slice. Specifically, this procedure involved thresholding for signal intensity ranges that captured the boundaries of WM and GM followed by visual inspection and manual editing to ensure that the WM and GM were properly defined. WM and GM volumes were determined three times for each specimen. WM:GM volume ratios of the total brain were also calculated three times. For the fetal measurements, native T2-weighted images were used because these images displayed better detail of structure edges than PD-weighted images, which was most likely a function of higher water content in fetal brains (Almajeed et al., 2004). For all dolphins, CSF volumes were not calcu-

lated because these measurements were most likely inaccurate due to postmortem leakage.

Cerebellum. WM and GM volumes of the cerebellum were determined after manually editing the label map of the whole brain, which had been generated previously. The WM and GM volumes of the cerebellum included the vermis and the cerebellar hemispheres but did not include the white or gray matter of the pons, the auditory nerve, the cochlear nucleus, trapezoid body, the lateral lemniscus white matter tracts, inferior olive, or spinal cord. WM and GM volumes were determined three times for each specimen. WM:GM volume ratios of the cerebellum were also calculated. For each specimen, the percentage of the brain occupied by the cerebellum was calculated by dividing the sum of the cerebellar WM and GM volumes by the sum of the total brain WM and GM volumes multiplied by 100. For the neonate, subadults, and adults, volumes from processed PD-weighted images were used. For fetuses, volumes from processed T2-weighted images were used.

Corpus callosum. The mid-sagittal area of the corpus callosum was determined by manually tracing the callosal perimeter of the midline sagittal section of both the "native" and "processed" sagittal PD images. The area was calculated using AMIRA software. During MR acquisition in the sagittal plane for each specimen, special care was taken to obtain MR images that would give an accurate longitudinal midline section. Therefore, during processing of the sagittal images, it was not necessary to perform any realignment. The mid-sagittal areas were determined three times from both the "native" and "processed" PD images. The areas obtained from the "native" PD images were favored because image processing decreased the resolution of images, as described previously. Mid-sagittal corpus callosum areas relative to the total brain weight (CCA/BW) were also calculated by dividing the area (from native PD-weighted images) by the total brain weight. The use of this ratio was useful, because it allowed a comparison with data from previous reports (Tarpley and Ridgway, 1994). However, this ratio mixes units by comparing an area to a mass. Therefore, when the ratio is used to compare across species, allometric scaling must be considered.

Hippocampus. Left and right hippocampal volumes were determined by manual segmentation of native, coronal T2-weighted images with the conventional MRI gray scale inverted (i.e., WM appears white and CSF appears black). The native images were used because of the higher resolution compared with the processed images (i.e., filtered and realigned). The T2-weighted images were used because they were better at highlighting fluid structures surrounding the hippocampus as compared to the PD images. These fluid structures served as boundaries of the hippocampus and were defined by higher signal intensities. Inverting the gray scale of the T2-weighted images (i.e., CSF now appears black rather than white) aided the manual segmentation of the hippocampus, because it sharpened the boundaries between the hippocampus and these fluid structures.

The anatomical landmarks and boundaries of the hippocampus used for the segmentation in this study were

based on the extensive description of the bottlenose dolphin hippocampus by Jacobs et al. (1979). Pantel et al. (2000) also served as a guide for segmenting the hippocampus. In most specimens, the hippocampal formation could be distinguished from other structures of the medial temporal lobe with sufficient accuracy to perform manual segmentation. The hippocampal formation refers to the assemblage of anatomical structures that includes the subiculum, Ammon's horn (hippocampus proper), and the dentate gyrus. In these MR images, the various structures of the hippocampal formation could not be adequately distinguished and were collectively grouped and referred to as the hippocampus.

Segmented volumes for the left and right hippocampal formations (i.e., hippocampus) were determined. The tracing of the hippocampal head started with the slice that first exhibited a distinct fluid spot (black in T2 with the conventional MRI gray scale inverted), which demarcated the posterior boundary of the amygdala. The medial boundary was the tentorium cerebelli and CSF of the subarachnoid space. The ventral and lateral boundaries were CSF of the parahippocampal sulcus. In the body of the hippocampus, CSF of the inferior horn of the lateral ventricle served as the lateral boundary, while the tentorium cerebelli and CSF of the subarachnoid space served as the medial boundary. The CSF of the parahippocampal sulcus served as the ventral boundary, while the CSF of the transverse fissure of Bichat and the fimbria (which was excluded) served as the dorsal boundary. In the tail of the hippocampus, the ascending crus of the fornix, the fimbria, and CSF of the inferior horn of the lateral ventricles served as the lateral boundary, while the tentorium cerebelli and CSF of the subarachnoid space served as the medial boundary. The CSF of the parahippocampal sulcus served as the ventral boundary, while the CSF of the transverse fissure of Bichat and the pulvinar of the thalamus served as the dorsal boundary.

Left and right hippocampus volumes were determined three times, separately. For each specimen, the percentage of brain occupied by the left or right hippocampus was calculated by dividing the hippocampus volume (from the native T2-weighted images) by the sum of the WM and GM volumes of the whole brain (i.e., from the processed PD-weighted images) multiplied by 100. The percentage of total brain WM occupied by the left or right hippocampus was calculated by dividing the hippocampus volume (from native T2-weighted images) by the WM volume of the whole brain (i.e., from processed PD-weighted images) multiplied by 100. The percentage of total brain GM occupied by the left or right hippocampus was calculated by dividing the hippocampus volume (from native T2-weighted images) by the GM volume of the whole brain (i.e., from processed PD-weighted images) multiplied by 100.

RESULTS

Volume Analysis Validation

Comparisons of expected and segmented volumes of water. The segmented volumes of water calculated from the native PD- and T2-weighted images closely approximated the expected volume (Table 2). The percent errors were less than 4%. The segmented volumes from processed PD- and T2-weighted images (with Gaussian filter application and subtraction) were more

TABLE 2. Comparisons of expected and segmented volumes of water

	Expected Volume (ml)	Segmented Volume (ml)	RMSE	% error
PD native ¹	19.8 ± 0.2	20.5 ± 0.6	0.9 ± 0.6	3.9 ± 2.4
PD Gauss 3x ²	19.8 ± 0.2	19.8 ± 0.3	0.2 ± 0.1	1.0 ± 0.4
PD Gauss 16x ³	19.8 ± 0.2	20.2 ± 0.2	0.4 ± 0.1	2.2 ± 0.3
PD Gauss 3x (realigned) ⁴	19.8 ± 0.2	19.7 ± 0.2	0.2 ± 0.1	0.9 ± 0.6
T2 native ⁵	19.8 ± 0.2	20.0 ± 0.3	0.6 ± 0.3	2.8 ± 1.3
T2 Gauss 3x ⁶	19.8 ± 0.2	19.8 ± 0.2	0.1 ± 0.0	0.5 ± 0.1
T2 Gauss 16x ⁷	19.8 ± 0.2	20.3 ± 0.1	0.6 ± 0.1	2.7 ± 0.5
T2 Gauss 3x (realigned) ⁸	19.8 ± 0.2	19.8 ± 0.2	0.1 ± 0.1	0.7 ± 0.2

N = 3 for each processing condition. Three replicate volume measurements were made. Volumes are reported as means and standard deviations.

¹Segmentation was completed using native (no Amira processing) PD-weighted images.

²A gauss filter (sigma=10; kernel=21) was applied to the PD native images three successive times. The results of the filter were then subtracted from the native PD images to acquire a new image set.

³A gauss filter (sigma=10; kernel=21) was applied to the PD native images sixteen successive times. The results of the filter were then subtracted from the native PD images to acquire a new image set.

⁴A gauss filter (sigma=10; kernel=21) was applied to the PD native images three successive times. The results of the filter were then subtracted from the native PD images to acquire a new image set. These images were then rotated 3° around the global y-axis.

⁵Segmentation was completed using native (no Amira processing) T2-weighted images.

⁶A gauss filter (sigma=10; kernel=21) was applied to the T2 native images three successive times. The results of the filter were then subtracted from the native T2 images to acquire a new image set.

⁷A gauss filter (sigma=10; kernel=21) was applied to the T2 native images sixteen successive times. The results of the filter were then subtracted from the native T2 images to acquire a new image set.

⁸A gauss filter (sigma=10; kernel=21) was applied to the T2 native images three successive times. The filter was then subtracted from the native T2 images to acquire a new image set. These images were then rotated 3° around the global y-axis.

accurate than the segmented volumes from native images (Table 2). Furthermore, realignment of both the PD- and T2-weighted images around the global y-axis (a technique used in threshold segmentation of specimens for symmetry of the left and right hemispheres) did not introduce any errors into the volume analysis.

Fetal brains were segmented into WM and GM from processed T2-weighted images; while subadult and adult brains were segmented from processed PD-weighted images (see Materials and Methods for explanation). Therefore, it was necessary to determine whether segmented volumes from processed PD images differed from segmented volumes from processed T2-weighted images. The results of this experiment revealed that the segmented volumes of water derived from PD- and T2-weighted images did not differ (Table 2).

Comparisons of expected and segmented volumes of brain tissue. Measurements of segmented volumes by computerized thresholding followed by manual editing were completed for the total cerebellum sample, the WM, and GM from both native and processed PD-weighted images (Table 3). In most cases, the segmented volumes from processed PD images were more accurate than the segmented volumes from native PD images (Table 3). For example, the segmented volumes of the cerebellum slice 1 indicated that the segmentation of the processed images contained smaller errors than the segmentation of the PD native images (total slice, 3.3% vs. 10.3%; WM, 5.5% vs. 8.3%; GM, 5.2% vs. 15.3%). However, a larger percent error was observed in

smaller segmented volumes. In general, for the segmented volumes of processed brain tissue, the total slice error was the lowest followed by WM and GM errors. These errors were larger than the errors in the water experiment, possibly because of the smaller volumes of brain tissue segmented compared with the volumes of water segmented. In addition, the error associated with the dissection of WM and GM may have caused the expected volume of WM and GM to be inaccurate. Additionally or alternatively, the larger errors of the segmented brain tissue may be linked to errors associated with measuring the water displaced by the tissue.

Comparisons of manual and threshold segmentation volumes. In all replicates, the manually segmented volumes from the native PD images were more similar to the threshold volumes (for WM and GM) derived from processed PD images than the threshold volumes derived from the native PD images (Table 4; Fig. 1). Thus, the processing of native PD images improved the accuracy of computerized threshold segmentation in determining the volumes of WM and GM. The processing of images (i.e., Gaussian filter application and subtraction) allowed a single threshold range to define the WM and GM for an entire slice (Fig. 1).

Brain Volumes

WM and GM segmented volumes of the total brain and cerebellum were determined for all dolphins except animals exhibiting gross brain pathologies and dolphins in which MRIs were of poor quality and deemed unsuit-

TABLE 3. Comparisons of expected and segmented volumes of brain tissue

	Total Slice				White matter				Gray matter			
	Expected volume (ml)	Segmented volume (ml)	RMSE	% error	Expected volume (ml)	Segmented volume (ml)	RMSE	% error	Expected volume (ml)	Segmented volume (ml)	RMSE	% error
Cerebellum slice 1:												
PD native ¹	7.0	7.7 ± 0.3	0.8	10.3 ± 4.3	3.0	2.9 ± 0.3	0.3	8.3 ± 4.7	4.0	4.6 ± 0.5	0.7	15.3 ± 11.6
PD filtered & realigned ²	7.0	7.2 ± 0.3	0.3	3.3 ± 4.6	3.0	3.0 ± 0.2	0.2	5.5 ± 2.3	4.0	4.0 ± 0.3	0.2	5.2 ± 2.5
Cerebellum slice 2:												
PD native ¹	2.5	2.5 ± 0.2	0.1	4.6 ± 3.5	1.5	1.4 ± 0.1	0.1	7.7 ± 3.5	1.0	1.0 ± 0.0	0.0	2.0 ± 1.6
PD filtered & realigned ²	2.5	2.6 ± 0.1	0.1	4.5 ± 3.7	1.5	1.4 ± 0.0	0.1	6.8 ± 2.0	1.0	1.1 ± 0.0	0.1	8.5 ± 3.0

Volumes are reported as means and standard deviations.

¹Segmentation was completed using native (no Amira processing) PD-weighted images.

²A gauss filter (sigma = 10; kernel = 21) was applied to the PD native images ten successive times. The results of the filter were then subtracted from the native PD images to acquire a new image set. These images were then rotated 2° around the global y-axis.

TABLE 4. A Comparison of manual segmentation volumes and threshold segmentation volumes of white matter and gray matter from native proton density (PD) and processed PD images

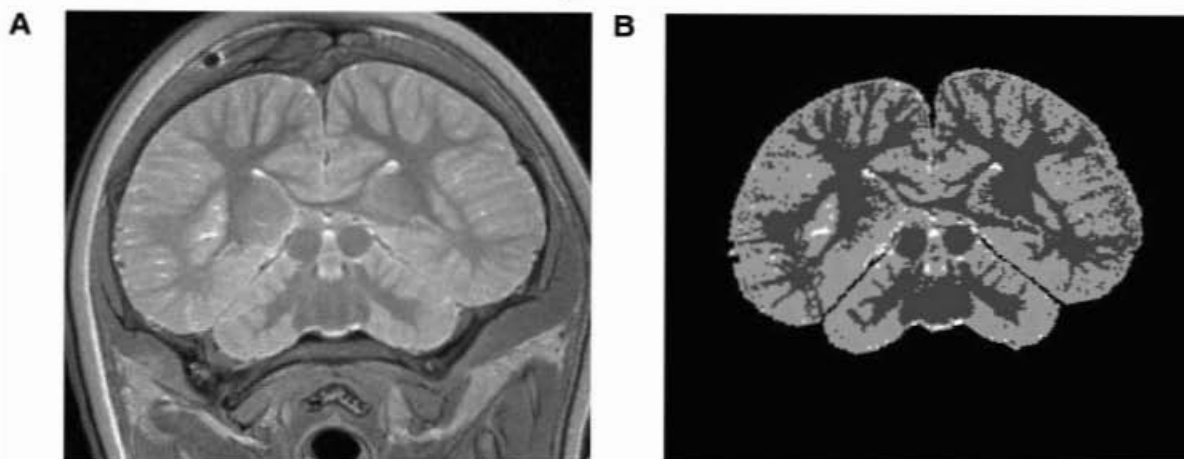
	White matter				Gray matter			
	Manual volume (ml)	Threshold volume (ml)	RMSE	% error	Manual volume (ml)	Threshold volume (ml)	RMSE	% error
CCSN05-040-La (section 35):								
PD native ¹	14.58 ± 0.37	12.21 ± 0.86	2.43	16.31 ± 4.51	18.43 ± 0.37	22.01 ± 3.74	4.60	19.32 ± 18.87
PD filtered ²	14.58 ± 0.37	15.84 ± 0.97	1.67	9.83 ± 7.54	18.43 ± 0.37	17.12 ± 1.01	1.72	7.85 ± 5.99
CCSN05-037-La (section 33):								
PD native ¹	12.52 ± 0.06	11.62 ± 2.74	2.38	16.89 ± 10.73	19.73 ± 0.03	20.66 ± 2.84	2.49	11.32 ± 7.00
PD filtered ²	12.52 ± 0.06	13.17 ± 1.55	1.64	8.02 ± 10.44	19.73 ± 0.03	18.78 ± 1.32	1.45	4.97 ± 6.63
CCSN05-231-La (section 30):								
PD native ¹	10.45 ± 0.03	9.34 ± 4.47	3.81	36.27 ± 5.46	13.39 ± 0.03	14.54 ± 4.59	3.92	29.00 ± 4.61
PD filtered ²	10.45 ± 0.03	10.35 ± 0.41	0.33	2.51 ± 2.35	13.39 ± 0.03	13.00 ± 0.45	0.52	3.41 ± 2.31

Volumes are reported as means and standard deviations.

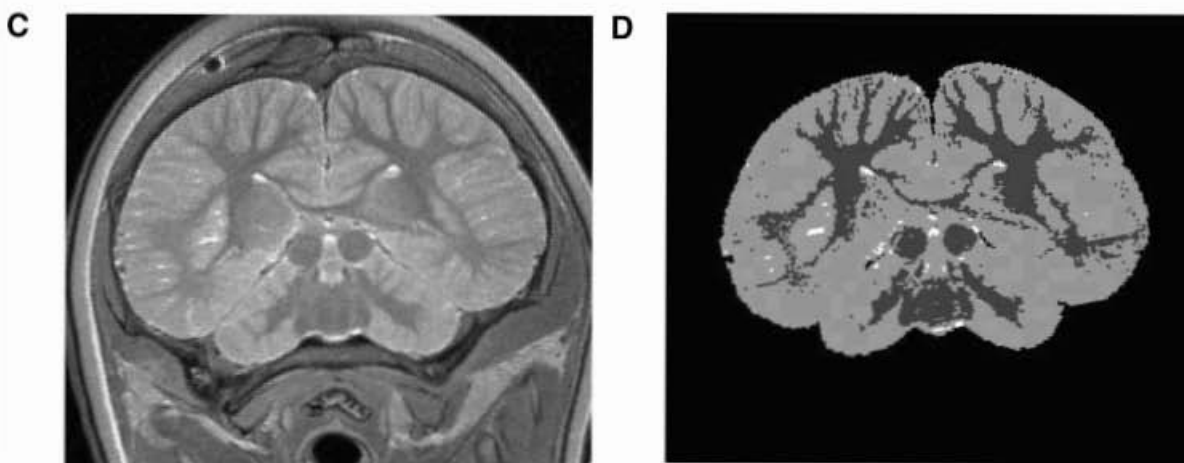
¹Segmentation was completed using native (no Amira processing) PD-weighted images.

²A gauss filter (sigma = 10; kernel = 21) was applied to the PD native images three successive times. The results of the filter were then subtracted from the native PD images to acquire a new image set.

Manual Segmentation from Native PD Images



Threshold Segmentation from Native PD Images



Threshold Segmentation from Processed PD Images

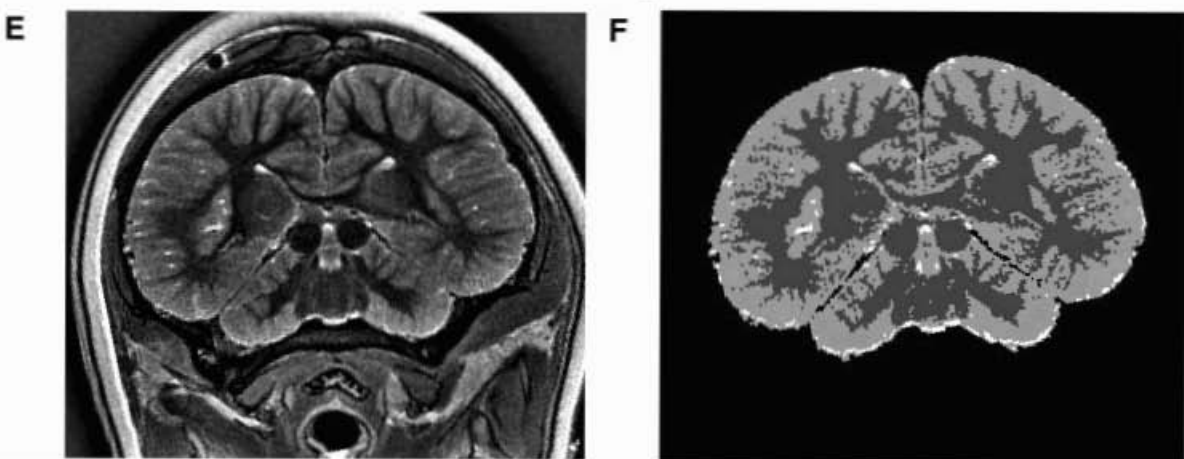


Fig. 1. A comparison between manual and threshold segmentation of native and processed images. The proton density- (PD) weighted label maps of white matter (WM), gray matter (GM), and cerebrospinal fluid (CSF) were from the same specimen at the level of the inferior and superior colliculus. For all dolphins, CSF volumes were not calculated because these measurements were most likely inaccurate due to

postmortem leakage. **A,B:** Manual segmentation from native PD images. **C,D:** Threshold segmentation from native PD images. **E,F:** Threshold segmentation from processed PD images. A, C, and E represent the nonsegmented image. B, D, and F represented the segmented label map of the brain that was removed from the head structure. WM is dark gray, GM is light gray, and CSF is white.

TABLE 5. Brain and cerebellum volumes of Atlantic white-sided dolphins

Field ID	Brain weight (g)	Brain volume (cm ³) ¹	Virtual brain weight (g) ²	Brain (cm ³) ³		Cerebellum (cm ³) ⁴		% of Brain ⁵
				WM	GM	WM:GM	WM	
CCSN04-195-La	1460.3	1439.9	1491.8	NA	NA	NA	NA	NA
				mean	NA	NA	NA	NA
				stdev	NA	NA	NA	NA
CCSN05-037-La	1292.2	1253.9	1299.0	467.04	718.55	0.66	53.17	113.67
				mean	53.17	0.13	3.38	2.00
				stdev	NA	NA	NA	NA
CCSN05-038-La	1153.0	NA	NA	NA	NA	NA	NA	NA
				mean	NA	NA	NA	NA
				stdev	NA	NA	NA	NA
CCSN05-039-La	1329.7	1293.6	1340.2	NA	NA	NA	NA	NA
				mean	NA	NA	NA	NA
				stdev	NA	NA	NA	NA
CCSN05-039-Fetus-La	65.4	63.0	65.2	11.25	48.21	0.23	0.62	3.85
				mean	1.58	0.05	0.06	0.03
				stdev	475.83	673.31	0.71	61.71
CCSN05-040-La	1305.3	1255.2	1300.3	33.98	41.66	0.10	3.69	8.76
				mean	32.35	0.38	3.41	6.57
				stdev	7.61	0.11	0.17	0.27
CCSN05-040-Fetus-La	131.9	127.9	132.5	413.20	561.29	0.74	37.25	103.80
				mean	38.49	0.11	3.60	4.64
				stdev	296.59	494.77	0.60	33.46
CCSN05-084-La	1057.8	1019.4	1056.1	30.35	26.16	0.09	1.98	4.71
				mean	NA	NA	NA	NA
				stdev	NA	NA	NA	NA
CCSN05-231-La	839.0	821.2	850.8	NA	NA	NA	NA	NA
				mean	NA	NA	NA	NA
				stdev	NA	NA	NA	NA
CCSN05-232-La	1186.1	NA	NA	NA	NA	NA	NA	NA
				mean	NA	NA	NA	NA
				stdev	NA	NA	NA	NA

¹Segmentation was completed from filtered and realigned PD weighted images.

²Virtual brain weight was calculated by multiplying the brain volume by the specific gravity of brain tissue or 1.036 g/cm³ (Stephan et al. 1981).

³Segmentation of brain into white matter (WM) and gray matter (GM) was completed from filtered and realigned T2 weighted images for fetuses and filtered and realigned PD weighted images for neonates, subadults, and adults.

⁴Segmentation of cerebellum into WM and GM was completed from filtered and realigned T2 weighted images for fetuses and filtered and realigned PD weighted images for neonates, subadults, and adults.

⁵Percentage of total brain occupied by the cerebellum = WM plus GM volumes of cerebellum divided by the WM plus GM volumes of the whole brain multiplied by 100%. For neonate, subadults, and adults, volumes from processed PD-weighted images were used. For fetuses, volumes from processed T2-weighted images were used. NA = data not available.

TABLE 6. The mid-sagittal area of the corpus callosum of Atlantic white-sided dolphins

Field ID		Corpus Callosum Area (mm ²) ¹		
		Native	Processed	CCA/BW ²
CCSN04-195-La	mean	129.08	130.91	0.088
	stdev	1.37	1.59	0.001
CCSN05-037-La	mean	NA	NA	NA
	stdev	NA	NA	NA
CCSN05-038-La	mean	NA	NA	NA
	stdev	NA	NA	NA
CCSN05-039-La	mean	156.10	153.81	0.117
	stdev	11.41	7.81	0.009
CCSN05-039-Fetus-La	mean	NA	NA	NA
	stdev	NA	NA	NA
CCSN05-040-La	mean	178.42	185.74	0.137
	stdev	0.88	9.68	0.001
CCSN05-040-Fetus-La	mean	NA	NA	NA
	stdev	NA	NA	NA
CCSN05-084-La	mean	130.97	132.12	0.124
	stdev	7.60	5.85	0.007
CCSN05-231-La	mean	113.96	100.49	0.136
	stdev	1.01	6.24	0.001
CCSN05-232-La	mean	NA	NA	NA
	stdev	NA	NA	NA

¹Manual segmentation of the corpus callosum was completed from native PD images and filtered-realigned PD images.

²CCA/BW = midsagittal area of the corpus callosum from native PD-weighted images divided by the brain weight (g). NA = data not available.

able for computerized thresholding (i.e., poor quality because of signal intensity loss of occipital lobes and cerebellum) (Table 5). The mid-sagittal area of the corpus callosum and hippocampus volumes were not determined in animals exhibiting gross brain pathologies (due to potential effects of the lesion on sizes of brain structures) and in the fetuses (due to poorer resolution of the fetal MRIs; Tables 6 and 7). The mid-sagittal area of the corpus callosum for CCSN05-037-La was not determined because the sagittal MRI did not provide an accurate midline section.

Total brain. Threshold segmentation of processed PD-weighted images was used to select for the brain surface (Fig. 2A). These segmentations were then used to calculate the total brain volume (Table 5). As expected, segmented volumes of the brain were strongly and significantly related to the total brain weight (Fig. 2B; R² = 0.9996).

A visual comparison of the degree of myelination of major white matter tracts among the MR images of a fetus, neonate, and adult brain at the level of the inferior and superior colliculi revealed an increase with development (Fig. 3A,C,E). Three-dimensional reconstructions of total white matter for these brains were created (Fig. 3B,D,F). The visual comparison of the degree of myelination among the dolphins of different age class categories was substantiated and quantified by the observed

TABLE 7. Hippocampus volumes of Atlantic white-sided dolphins

Field ID		L. Hippocampus				R. Hippocampus			
		(mm ³) ¹	% of Brain ²	% of WM ³	% of GM ⁴	(mm ³) ¹	% of Brain ²	% of WM ³	% of GM ⁴
CCSN04-195-La	mean	751.96	NA	NA	NA	887.66	NA	NA	NA
	stdev	21.91	NA	NA	NA	4.45	NA	NA	NA
CCSN05-037-La	mean	868.32	0.073	0.188	0.121	736.49	0.062	0.162	0.102
	stdev	112.54	0.010	0.035	0.020	108.97	0.010	0.048	0.009
CCSN05-038-La	mean	NA	NA	NA	NA	NA	NA	NA	NA
	stdev	NA	NA	NA	NA	NA	NA	NA	NA
CCSN05-039-La	mean	927.47	NA	NA	NA	745.84	NA	NA	NA
	stdev	135.77	NA	NA	NA	119.55	NA	NA	NA
CCSN05-039-Fetus-La	mean	NA	NA	NA	NA	NA	NA	NA	NA
	stdev	NA	NA	NA	NA	NA	NA	NA	NA
CCSN05-040-La	mean	1043.55	0.091	0.219	0.156	861.32	0.075	0.180	0.129
	stdev	112.31	0.010	0.008	0.026	173.62	0.015	0.023	0.034
CCSN05-040-Fetus-La	mean	NA	NA	NA	NA	NA	NA	NA	NA
	stdev	NA	NA	NA	NA	NA	NA	NA	NA
CCSN05-084-La	mean	923.99	0.095	0.226	0.164	967.93	0.099	0.236	0.173
	stdev	133.69	0.014	0.047	0.021	68.02	0.007	0.035	0.010
CCSN05-231-La	mean	544.32	0.069	0.184	0.110	462.29	0.058	0.157	0.094
	stdev	24.94	0.003	0.014	0.010	24.42	0.003	0.015	0.008
CCSN05-232-La	mean	NA	NA	NA	NA	NA	NA	NA	NA
	stdev	NA	NA	NA	NA	NA	NA	NA	NA

¹Manual segmentation of hippocampus was completed on native T2 images.

²Percentage of total brain occupied by the left or right hippocampus = left or right hippocampus volume (from native T2 weighted images) divided by the white matter (WM) plus gray matter (GM) volumes of the whole brain (from processed PD weighted images) multiplied by 100%.

³Percentage of total brain WM occupied by the left or right hippocampus = left or right hippocampus volume (from native T2 weighted images) divided by the WM of the whole brain (from processed PD weighted images) multiplied by 100%.

⁴Percentage of total brain GM occupied by the left or right hippocampus = left or right hippocampus volume (from native T2 weighted images) divided by the GM of the whole brain (from processed PD weighted images) multiplied by 100%. NA = data not available

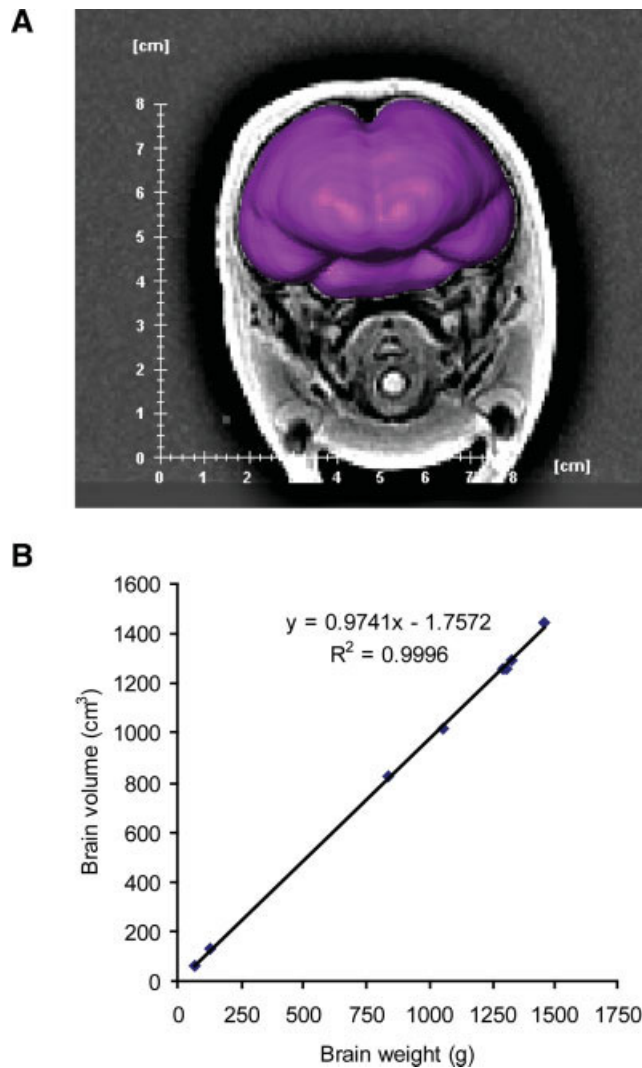


Fig. 2. **A:** Three-dimensional reconstruction of fetal brain surface (CCSN05-039-fetus-La). **B:** Measured brain volume (cm^3) vs. actual brain weight (g).

increase in WM:GM volume ratios with increasing body length (Table 5; Fig. 4A).

Cerebellum. A visual comparison of the degree of myelination of major white matter tracts among the MR images of a fetus, neonate, and adult cerebellum at the level of the inferior and superior colliculi also revealed an increase in white matter tracts with development (Fig. 3). These observations were substantiated and quantified by the increase in WM:GM volume ratios of the cerebellum with increasing body length (Table 5; Fig. 4B). However, the larger fetus (CCSN05-040-Fetus-La) had a WM:GM volume ratio approximately equivalent to that of the subadults and adults. In addition, the GM segmented volumes of the cerebellum increased with length for both males and females (Fig. 5).

Corpus callosum. The mid-sagittal area of the corpus callosum ranged between 113.96 and 178.42 mm^2 (Table 5). The corpus callosum area (mm^2) to brain mass

(g) ratio (CCA/BM) ranged between 0.088 and 0.137 (Table 5). The mid-sagittal area of the corpus callosum in adult females was larger than that of the neonate dolphin (Fig. 6).

Hippocampus. In all postmortem MRI scans of Atlantic white-sided dolphins in this study, the hippocampus was identified. The hippocampus was located in the medial wall of the temporal lobes, as visible from 3D reconstructions of the total white matter and the hippocampus (Fig. 7). In the adult specimen brain CCSN05-040-La, the brain measured 12.7 cm from the anterior border of the frontal lobe to the posterior border of the occipital lobe. The anterior border of the hippocampus started at 7.3 cm from the anterior border of the frontal lobe. The boundaries of the hippocampus were best observed in native T2-weighted images, rather than the PD-weighted images. This finding can be best explained by the cerebrospinal fluid surrounding this structure, as observed by the hyperintensity of the inferior horn of the lateral ventricle (lateral border), the hyperintensity of the parahippocampal sulcus (ventral border), and the hyperintensity of the subarachnoid space (the medial and dorsal borders; Fig. 8A–F).

In the Atlantic white-sided dolphins in this study, the left hippocampus ranged from 0.544 to 1.043 cm^3 ; the right hippocampus ranged from 0.462 to 0.967 cm^3 . The hippocampi of adult females were larger than that of the neonate female (Fig. 8G,H). Furthermore, the neonate hippocampus contained more fluid in the inferior horn of the lateral ventricle, the transverse fissure of Bichat, and within the hippocampus itself (Fig. 8A–F).

DISCUSSION

This study presents a quantitative approach to determining the size of brain structures from in situ MR images of freshly dead, Atlantic white-sided dolphins. We present WM and GM volumes, as well as WM:GM volume ratios of the total brain and cerebellum along an ontogenetic series from fetus to adult. These data provide a quantitative measurement of the degree of myelination of white-matter tracts during ontogeny. In addition, the mid-sagittal area of the corpus callosum and hippocampus volumes were determined. The measurements of WM, GM, and hippocampus volumes are the first to be reported for any cetacean species.

Myelination Patterns During Ontogenesis

MRI and volumetric analysis of MRI data sets have been used to study brain development in humans, as reviewed by Inder and Huppi (2000) and Lenroot and Giedd (2006). Specifically, MRI has been used to study the myelination of axons, a critical phase during brain development. Immature white matter is composed of axons that do not contain myelin or mature myelin sheaths. Immature white matter displays a higher signal on T2-weighted images compared with mature white matter, with longer T2 relaxation times than those of the adult brain, predominantly due to the higher water content of immature white matter (Holland et al., 1986; McArdle et al., 1987; Barkovich et al., 1988). With increasing maturation of the brain, the white matter signal decreases on T2-weighted images. This signal loss

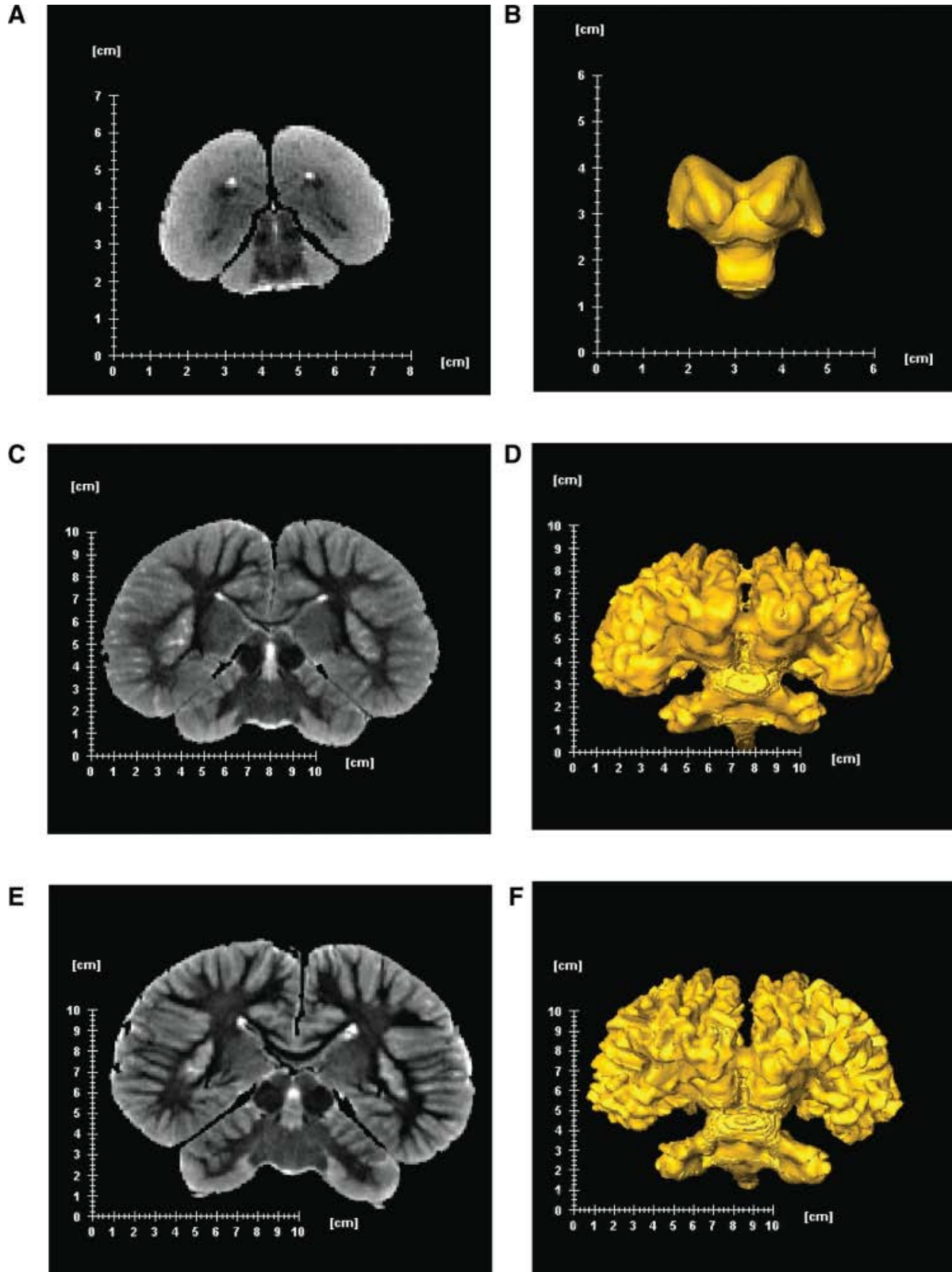


Fig. 3. A visual comparison of the degree of myelination (i.e., white matter tracts) during ontogeny. **A,B:** Fetal specimen CCSN05-039-Fetus-La. **C,D:** Neonate specimen CCSN05-231-La. **E,F:** Adult specimen CCSN05-040-La. All brain magnetic resonance sections are at

the level of the inferior and superior colliculi. The panels to the right represent three-dimensional reconstructions of the white matter of the entire brain.

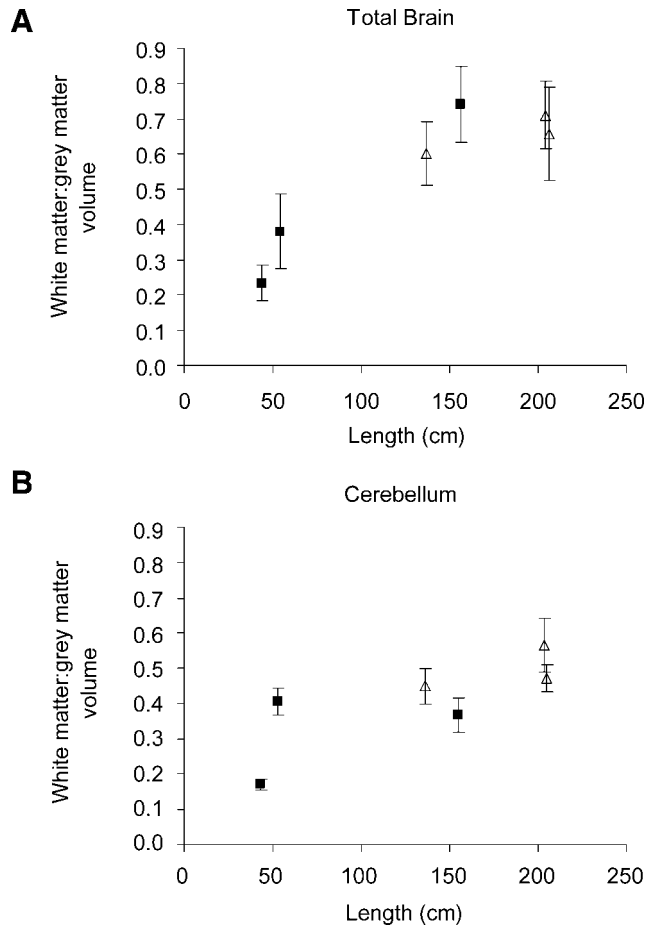


Fig. 4. A quantitative comparison of the degree of myelination (i.e., white matter tracts) during ontogeny. **A:** White matter (WM): gray matter (GM) volume ratios of the total brain vs. length. **B:** WM:GM volume ratios of the cerebellum vs. length (cm). Males = black squares; females = open triangles.

correlates with anatomical myelination determined by histological analysis, as discussed by Inder and Huppi (2000). However, the pattern of T2-weighted images can lag some weeks behind the histological timetable and may require a threshold of myelin to change the signal intensity, as reviewed by Inder and Huppi (2000). Although a comparison of myelination using histological analysis vs. T2-weighted sequences has not been completed in cetaceans, we expect the histological and the T2-weighted timetables in cetaceans to be similar to that of humans.

In this study, we used MRI to investigate the changes of myelination during brain development of the Atlantic white-sided dolphin by calculating the volumetric changes of WM and GM during ontogeny. More specifically, WM measurements represented myelinated or mature white matter volumes; GM measurements represented the sum of immature white matter, cortical gray matter, and subcortical gray matter volumes. To our knowledge, white matter and gray matter volumes have not been reported previously in any cetacean species. The WM:GM volume ratios of the entire brain increased from the fetus to adult in the Atlantic white-sided dol-

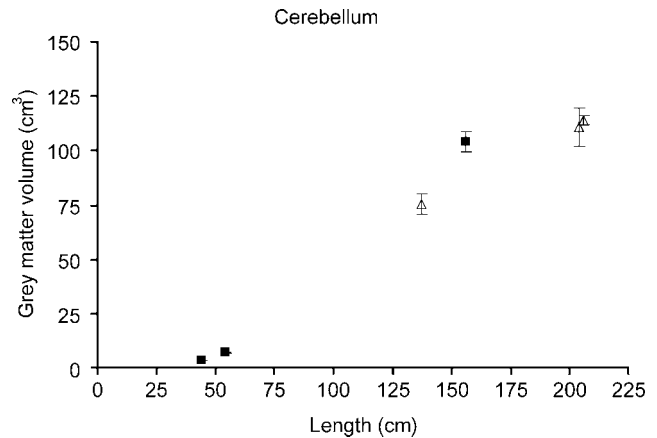


Fig. 5. Volumes (cm^3) of the cerebellum gray matter vs. length (cm). Males = black squares; females = open triangles.

phin brain, representing an increase in myelination during ontogeny (Fig. 4). This pattern is similar to what is observed in humans, as discussed by Inder and Huppi (2000) and Lenroot and Giedd (2006).

In the Atlantic white-sided dolphins used in this study, myelination advanced at different rates in different regions of the brain. The white matter tracts of the fetal hindbrain and cerebellum were prominent (Figs. 3, 4). However, in the telencephalon, the white matter tracts were far less developed. The white matter tracts in the center of the fetal cerebral hemispheres were more myelinated than the white matter tracts located more peripherally (Fig. 3). In addition, the white matter tracts of the auditory pathways in the fetal brains were myelinated, indicated by the T2 hypointensity signal of the inferior colliculus, the cochlear nuclei, and trapezoid body. These findings provide evidence that hearing and auditory processing regions develop early during cetacean ontogeny, as described in previous odontocete studies (Solntseva, 1999).

These findings are similar to the patterns of myelination observed during the development of the human brain. In humans, myelination begins in the third trimester and continues well after birth (Hayman et al., 1992). At 29 weeks, myelination begins with the brainstem and then continues from inferior to superior and posterior to anterior (Inder and Huppi, 2000). During this time period, myelin is abundant in the central auditory pathway including the proximal end of the cochlear nerve, trapezoid body, lateral lemniscus, and the inferior colliculus (Moore et al., 1995). Interestingly, the auditory blink-startle response and auditory brainstem response (ABR) indicate that responses to an acoustic stimulus could be recorded from a 29-week-old fetus, as discussed by Moore et al. (1995). At 37–40 weeks postconception, myelin is present in the lateral cerebellar white matter (Inder and Huppi, 2000). In contrast, microscopic myelin is not present in the white matter of the frontal and occipital lobes until 47–50 weeks (Inder and Huppi, 2000). The white matter tracts in the center of the cerebral hemispheres become myelinated before the white matter tracts located more peripherally (Inder and Huppi, 2000), similar to what was observed in Atlantic white-sided dolphins.

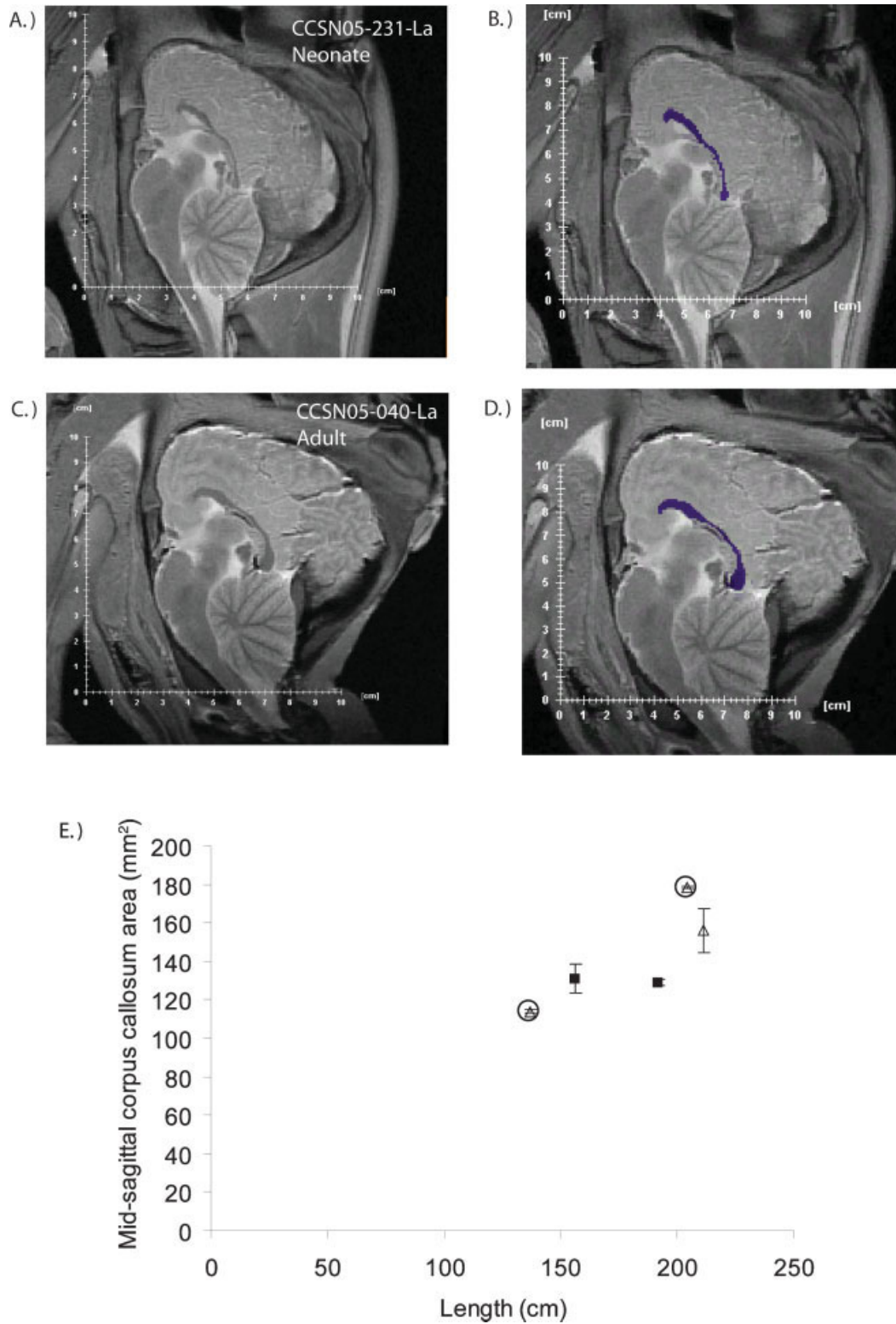


Fig. 6. Segmentation label maps and mid-sagittal areas of the corpus callosum. **A:** Mid-sagittal section for the neonate specimen CCSN05-231-La. **B:** Pixels selected to calculate the mid-sagittal area of the corpus callosum for the neonate specimen CCSN05-231-La. **C:** Mid-sagittal section for the adult specimen CCSN05-040-La. **D:** Pixels

selected to calculate the mid-sagittal area of the corpus callosum for the adult specimen CCSN05-040-La. Selected area = purple. **E:** Mid-sagittal area of the corpus callosum (mm²) vs. length (cm). CCSN05-231-La and CCSN05-040-La data points are encircled. Males = black squares; females = open triangles.

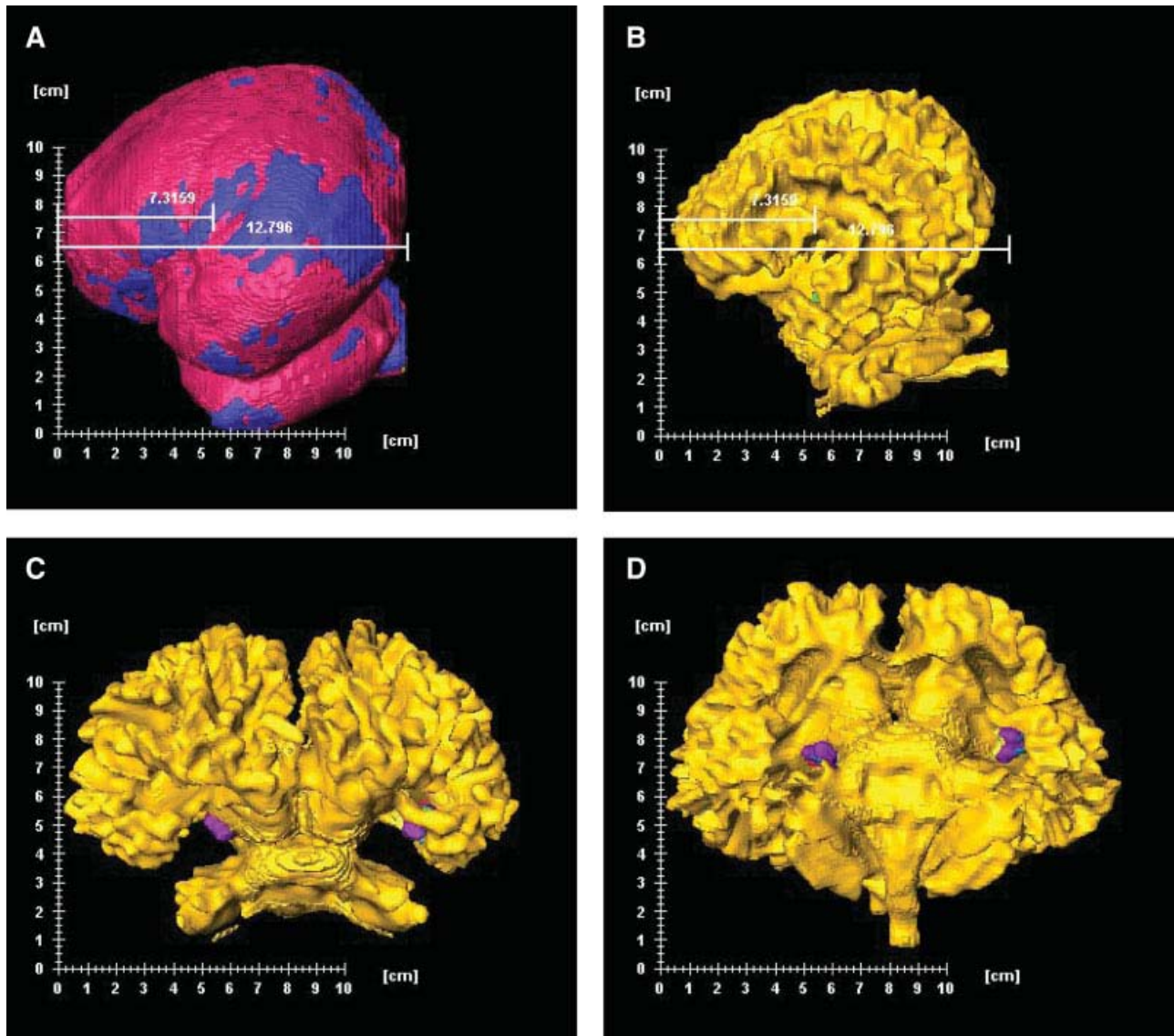


Fig. 7. Three-dimensional reconstructions of the adult specimen brain CCSN05-040-La illustrating the spatial relationship of the hippocampus with the rest of the brain. **A:** A sagittal view of the three-dimensional reconstruction of the brain. Surface of brain = red; cerebrospinal fluid (CSF) = blue. The brain measured 12.7 cm from the anterior border of the frontal lobe to the posterior border of the occipital lobe (bottom line). The anterior border of the hippocampus started at 7.3 cm from the anterior border of the frontal lobe (top line). **B:** A

sagittal view of the three-dimensional reconstruction of the white matter with the gray matter and CSF stripped away. The CSF of the lateral ventricle abutting the hippocampus is visible (green). **C:** Anterior view of the white matter and hippocampus. **D:** Ventral view of the white matter and hippocampus. White matter = yellow; hippocampus = purple; fimbria = red; CSF of the parahippocampal sulcus abutting the hippocampus = blue; CSF of lateral ventricle abutting the hippocampus = green.

Measurements of Brain Structures

Cerebellum. The large cerebellum in Atlantic white-sided dolphins, measured in this study from in situ MR images, is consistent with previous findings on the cerebellum in other delphinid species (Ridgway, 1990; Marino et al., 2000). In our study, the cerebellum (WM and GM volumes combined) of subadult and adult specimens ranged between 13.8 to 15.0% of the total brain size. These findings were within the range of measurements made from MR images of dissected and formalin-fixed brains of bottlenose dolphins and common dolphins

(Marino et al., 2000). For Atlantic white-sided, bottlenose, and common dolphins, the cerebellum, which averages approximately 15% of the total brain size, is relatively much larger than that of humans (10.3%) and some non-human primates (9.2% for Cercopithecidae, i.e., baboons, rhesus monkeys, and mangabeys; and 9.3% for Cebidae, i.e., cebus and squirrel monkeys; Marino et al., 2000).

Why do dolphins have such a large cerebellum? In reviewing the evidence, Marino et al. (2000) and Ridgway (1990) suggest that the cerebellum may play an important role in acoustic processing, in addition to its function in the control and coordination of movements. This specu-

CCSN05-231-La: Neonate



CCSN05-040-La: Adult

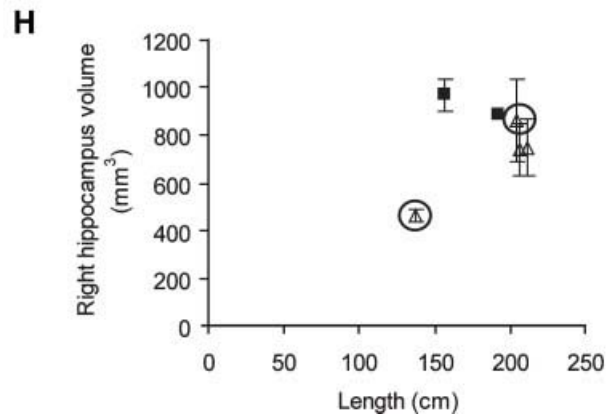
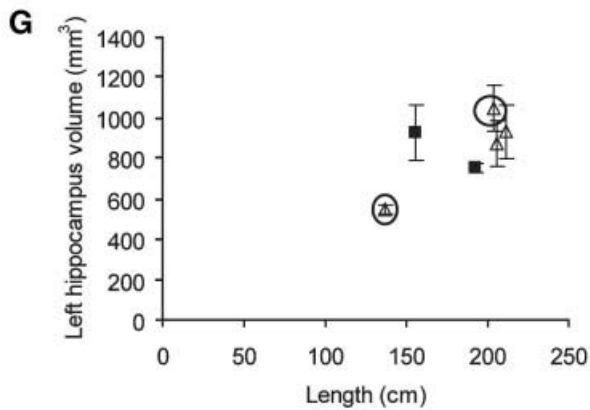
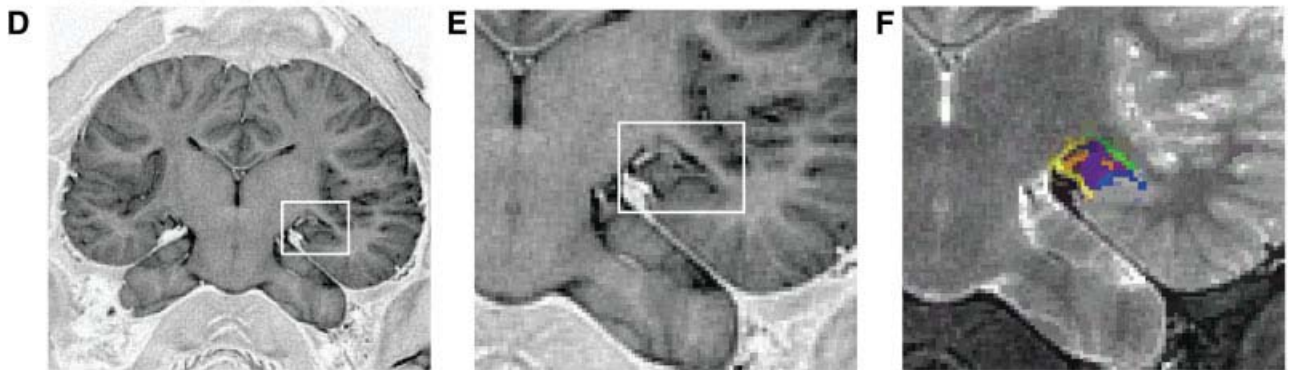


Fig. 8. Segmentation label maps and volumes of the hippocampus. **A–C:** Hippocampus of neonate specimen CCSN05-231-La. **D–F:** Hippocampus of adult specimen CCSN05-040-La. A and D demarcate the position of the left hippocampus in the medial wall of the temporal lobe. The hippocampus is highlighted with a white box in the native T2-weighted images with the conventional magnetic resonance imaging (MRI) gray scale inverted. B and E are an enlargement of A and D, respectively. C and F show the hippocampus segmentation in native T2-weighted images (normal MRI gray scale), which allow better visibility of selected pixels that represent different brain structures. Hippocampus = purple; cerebrospinal fluid (CSF) of the inferior horn

of the lateral ventricle = green; CSF of the parahippocampal sulcus = blue; CSF of the subarachnoid space and the transverse fissure of Bichat = yellow; hippocampal fluid = orange. **G:** Volume of the left hippocampus (mm³) vs. length (cm). **H:** Volume of the right hippocampus (mm³) vs. length (cm). Volumes were determined by manual segmentation of native, coronal T2-weighted images with the conventional MRI gray scale inverted such as shown in B and E. The results of segmentation are shown in C and F. CCSN05-231-La and CCSN05-040-La data points are encircled. Males = black squares; females = open triangles.

lation is based on the findings in echolocating bats, as discussed by Marino et al. (2000). For example, in the big brown bat (*Eptesicus fuscus*), cerebellar neurons function in representation of sound location (Kamada and Jen, 1990). In addition, qualitative observations of the paramedian lobules and paraflocculus of echolocating odontocetes reveal that these regions of the cerebellum are expanded (Ridgway, 1990). These brain structures are more enlarged in echolocating bats as compared to non-echolocating bats, as discussed by Marino et al. (2000). Similarly, there is a huge expansion of the cerebellum of Mormyrid electric fishes in which this structure functions in the localization of objects by the distortion of electric fields (Bullock and Heiligenberg, 1986).

Corpus callosum. The small corpus callosum that we measured in Atlantic white-sided dolphins from in situ MR images is consistent with previous observations of corpus callosum size in dissected and formalin-fixed brains of other odontocete species (Tarpley and Ridgway, 1994). In our study, the corpus callosum area (mm^2) to brain mass (g) ratio (CCA/BM) ranged between 0.088 and 0.137. These CCA/BM ratios were within the range of measurements found in other odontocete studies (Tarpley and Ridgway, 1994). For example, the bottlenose dolphin has a CCA/BM ratio range of 0.143 to 0.227 ($N = 15$), whereas the Pacific white-sided dolphin has a CCA/BM ratio range of 0.159 to 0.198 ($N = 3$).

The CCA/BM ratio is much smaller in odontocetes than in most other mammals, including humans, in which the CCA/BM ratio is approximately 0.9 (Tarpley and Ridgway, 1994). Although some of this difference may be a function of differences in body size, it may also reflect differences in the function of the corpus callosum. The corpus callosum plays a key role in transferring information between the two hemispheres including unification of sensory fields, memory storage and retrieval, attention and arousal, enhancing language and auditory functions, as summarized by Lenroot and Giedd (2006). Ridgway (1990) suggested that the smaller corpus callosum area in odontocetes would result in greater hemispheric independence. In fact, recordings of brain activity of the bottlenose dolphin revealed that the cerebral hemispheres can produce electroencephalograph waveforms indicative of wakefulness in one hemisphere and sleep in the opposite hemisphere (Mukhametov et al., 1977). Ridgway and Tarpley (1994) suggest that hemispheric independence (for whatever reasons) in cetaceans may have been favored during evolution, despite the evolutionary pressure for interhemispheric coordination and asymmetry in movement patterns of the body.

Hippocampus. To date, MRI studies of odontocete brains that were removed and preserved in formalin have been unable to identify the hippocampus, except in the killer whale (Marino et al., 2001a-c, 2003a,b, 2004a,b). In all postmortem MRI scans of Atlantic white-sided dolphins in the current study, the hippocampus was identified. The hippocampus was located more in the medial wall of the temporal lobes, similar to what has been observed in traditional histological studies of bottlenose dolphins (Jacobs et al., 1979).

It is possible that the key factor in finding the hippocampus in odontocete MR images is performing the imaging of the brain in situ (Montie et al., 2007). The hippo-

campus was located by recognizing the surrounding fluid structures (Fig. 8). These boundaries were the CSF of the inferior horn of the lateral ventricle, the parahippocampal sulcus, and the transverse fissure of Bichat. These structures were best observed in native T2-weighted images rather than PD-weighted images because of the hyperintensity of fluid. It is possible that severing the head and removing the brain, as was done in previous delphinid MRI studies, leads to excessive leakage of CSF and therefore reduces the ability to perceive the hippocampus boundaries. This possibility, in conjunction with the weight of the brain on the hippocampus and its potential thinning in the dorsal-ventral direction, may impede the visual perception of the hippocampal formation from MR images of formalin-fixed brains.

Hippocampal volumes in cetaceans have not been reported previously. However, the small hippocampus in the Atlantic white-sided dolphin specimens that we measured from MR images is consistent with previous qualitative findings on hippocampus size in the bottlenose dolphin (Jacobs et al., 1979). Compared with the carnivora and ungulates, the hippocampus in cetaceans is considerably reduced, except for the ventral portion near the temporal lobes. When the hippocampus of a bottlenose dolphin was compared with that in a human brain of the same size and weight, transverse sections at the histological level revealed that the dolphin hippocampus was smaller (Jacobs et al., 1979). In a group of human subjects with a mean age of 20.4 (± 2.2) years, Pantel et al. (2000) found the mean volume of the hippocampal formation to be 1.975 cm^3 in the left hemisphere and 1.987 cm^3 in the right hemisphere. In our study, the left hippocampus ranged from 0.544 to 1.043 cm^3 ; the right hippocampus ranged from 0.462 to 0.967 cm^3 . Given the small volume of the hippocampus observed in this study and humans, future research studies should use a 3 T MRI scanner to provide images of better resolution than images acquired from a 1.5 T scanner. The segmentation from 3 T images would provide more precise measurements of the hippocampus.

The mammalian hippocampus is required for some aspects of spatial learning and memory. O'Keefe and Nadel (1978) proposed that activity of hippocampal neurons together represent a cognitive map of our surroundings. Recently, the brains of humans with extensive navigation experience (i.e., licensed London taxi drivers) were found to exhibit an enlarged posterior hippocampus compared with control subjects, as observed from structural MRI and voxel-based morphometry (i.e., segmentation; Maguire et al., 2000). In odontocetes, the role of the hippocampus in spatial navigation is not known. However, given the evidence for well-developed long-term memory capacities in dolphins (Herman and Gordon, 1974; Thompson and Herman, 1977) and prodigious memory-based navigational abilities in other cetaceans (Baker et al., 1986; Calambokidis et al., 2001), it might be postulated that cetacean spatial and long-term memory is dependent on extrahippocampal structures (Oelschlager and Oelschlager, 2002; Marino et al., 2007).

Implications: Relationships Between Brain Structure Size and Environmental Chemicals

The ability to determine the volumes of brain structures in cetaceans from in situ MR images may provide

a more accurate and quantitative approach than traditional dissection techniques. The volumetric measurements can be used not only in comparative neuroanatomy and neurodevelopment studies but also to investigate how marine biotoxins and anthropogenic pollutants affect the central nervous system in cetaceans and other marine mammal species. These natural toxins and environmental pollutants are emerging threats to marine mammal health and may affect the size of sensitive brain structures. For example, domoic acid (a type of biotoxin produced by some diatom *Pseudo-nitzschia* species and associated with harmful algal blooms) has been shown to cause hippocampal atrophy in California sea lions (Silvagni et al., 2005). Using the approach outlined in this study, the hippocampus of sea lions exposed to domoic acid could be measured from in situ MR images and compared with healthy individuals. A similar approach has been used recently to investigate possible neuroanatomical changes in humans exposed to organophosphate nerve agents (Heaton et al., 2007).

Of particular concern in odontocetes is the bioaccumulation of PCBs and PBDEs that interfere with thyroid hormone-dependent neurodevelopment. For example, in mouse cerebellar culture assays, OH-PCBs have been shown to inhibit thyroid hormone-dependent arborization of cerebellar Purkinje cell dendrites (Kimura-Kuroda et al., 2005). The dendrites exhibited poor growth and the secondary branches shrunk, which significantly decreased the dendritic area of the Purkinje cells. Because the dendrites of the Purkinje cells comprise the bulk of the cerebellum gray matter, we hypothesize that the gray matter volumes of the cerebellum of dolphins exposed to higher levels of thyroid hormone-disrupting chemicals (THDCs) during development would be smaller than those of animals with lower concentrations of THDCs. In addition, Sharlin et al. (2006) observed that in fetal rats, exposure to Aroclor 1254 (a PCB mixture) decreases the cell density of the corpus callosum in a manner similar but not identical to hypothyroidism. Hence, we hypothesize that neonate and subadult dolphins that contain high levels of THDCs will have a smaller corpus callosum area than those individuals with lower concentrations of THDCs. In the current study, we have established an approach to test these hypotheses.

Because odontocetes live in a niche in the marine environment that is analogous to the human niche in the terrestrial environment (i.e., apex predators), understanding the impacts of thyroid hormone disrupting chemicals on neurodevelopment in cetaceans can help to understand the potential effects of these chemicals on children's health. In addition, the fact that odontocetes bioaccumulate the highest levels of persistent organic pollutants of any living species on our planet and transfer a majority of this chemical burden to their first-born calves (Wells et al., 2005) makes odontocetes an important "real world" animal model that may give us insight in investigating this health risk in humans.

ACKNOWLEDGMENTS

We thank the following past and present members of the Cape Cod Stranding Network for coordination and collection of specimens: Kristen Patchett, Betty Lentell, Brian Sharp, Kate Swails, Sarah Herzig, and Trish

O'Callaghan. We are particularly thankful to Andrea Bogomolni and Dr. Michael Moore for assistance in necropsies. We are especially thankful to Scott Garvin, Rick Rupan, Dr. Tin Klanjscek, Dr. Gareth Lawson, Dr. Regina Campbell-Malone, Dr. Joy Lapsertitis, Paul Ryan Craddock, Tim Cole, Brendan Hurley, Misty Nelson, Brenda Rone, Brett Hayward, and Misty Niemeyer for assistance during specimen preparation and necropsies. We are especially thankful to Dr. Steven Sweriduk for allowing the use of the MRI scanner at Shields MRI and CT of Cape Cod. We are indebted to Julie Arruda, Scott Cramer, Dr. Iris Fischer, Bill Perrault, Terri Plifka, Cheryl Loring, and Rose Pearson for assistance during MR imaging of specimens and data processing. We also thank Greg Early and Dr. Mark Baumgartner for helpful discussions. This study was conducted under a letter of authorization from Dana Hartley and the National Marine Fisheries Service Northeast Region, which allowed the possession of marine mammal parts. E.M. was funded through an Environmental Protection Agency STAR fellowship, a National Woman's Farm and Garden Association Scholarship, Woods Hole Oceanographic Institution, Sawyer Endowment, and Walter A. and Hope Noyes Smith.

LITERATURE CITED

- Almajeed AA, Adamsbaum C, Langevin F. 2004. Myelin characterization of fetal brain with mono-point estimated T1-maps. *Magn Reson Imaging* 22:565-572.
- Baker CS, Herman LM, Perry A, Lawton WS, Straley JM, Wolman AA, Kaufman GD, Winn HE, Hall JD, Reinke JM, Ostman J. 1986. Migratory movement and population structure of humpback whales (*Megaptera novaeangliae*) in the central and eastern North Pacific. *Mar Ecol Prog Ser* 31:105-119.
- Barkovich AJ, Kjos BO, Jackson DE, Norman D. 1988. Normal maturation of the neonatal and infant brain: MR imaging at 1.5T. *Radiology* 166:173-180.
- Bullock TH, Heiligenberg W. 1986. *Electroreception*. New York: Wiley.
- Calambokidis J, Steiger GH, Straley JM, Herman LM, Cerchio S, Salden DR, Urban RJ, Jacobsen JK, von Ziegler O, Balcomb KC, Gabriele CM, Dahlheim ME, Uchida S, Ellis G, Miyamura Y, De Guevara PPL, Yamaguchi M, Sato F, Mizroch SA, Schlender L, Rasmussen K, Barlow J, Quinn IITJ. 2001. Movements and population structure of humpback whales in the North Pacific. *Mar Mammal Sci* 17:769-794.
- De Boer J, Wester PG, Klamer HJ, Lewis WE, Boon JP. 1998. Do flame retardants threaten ocean life? *Nature* 394:28-29.
- Evans AC, Brain Development Cooperative Group. 2006. The NIH MRI study of normal brain development. *Neuroimage* 30:184-202.
- Hayman LA, McArdle CB, Shah YP. 1992. Neonatal brain. *Clin Imaging* 2:45-52.
- Heaton KJ, Palumbo CL, Proctor SP, Killiany RJ, Yurgelun-Todd DA, White RF. 2007. Quantitative magnetic resonance brain imaging in US army veterans of the 1991 Gulf War potentially exposed to sarin and cyclosarin. *Neurotoxicology* 28:761-769.
- Herman LM, Gordon JA. 1974. Auditory delayed matching in the bottlenose dolphin. *J Exp Anal Behav* 21:19-26.
- Holland BA, Haas DK, Norman D, Brant-Zawadzki M, Newton TH. 1986. MRI of normal brain maturation. *AJR Am J Neuroradiol* 7:201-208.
- Houde M, Pacepavicius G, Wells RS, Fair PA, Letcher RJ, Alaei M, Bossart GD, Hohn AA, Sweeney J, Solomon KR, Muir DCG. 2006. Polychlorinated biphenyls (PCBs) and hydroxylated polychlorinated biphenyls (OH-PCBs) in plasma of bottlenose dolphins (*Tursiops truncatus*) from the Western Atlantic and the Gulf of Mexico. *Environ Sci Technol* 40:5860-5866.

- Inder TE, Huppi PS. 2000. In vivo studies of brain development by magnetic resonance techniques. *Ment Retard Dev Disabil Res Rev* 6:59–67.
- Jacobs MS, McFarland WL, Morgane PJ. 1979. The anatomy of the brain of the bottlenose dolphin (*Tursiops truncatus*). Rhinic lobe (Rhinecephalon): the archicortex. *Brain Res Bull* 4:1–108.
- Kamada T, Jen PH. 1990. Auditory response properties and direction sensitivity of cerebellar neurons of the echolocating bat, *Eptesicus fuscus*. *Brain Res* 528:123–129.
- Kimura-Kuroda J, Nagata I, Kuroda Y. 2005. Hydroxylated metabolites of polychlorinated biphenyls inhibit thyroid-hormone-dependent extension of cerebellar purkinje cell dendrites. *Dev Brain Res* 154:259–263.
- Lenroot RK, Giedd JN. 2006. Brain development in children and adolescents: insights from anatomical magnetic resonance imaging. *Neurosci Biobehav Rev* 30:718–729.
- Maguire EA, Gadian DG, Johnsrude IS, Good CD, Ashburner J, Frackowiak RSJ, Firth CD. 2000. Navigation-related structural change in the hippocampi of taxi drivers. *Proc Natl Acad Sci USA* 97:4398–4403.
- Marino L. 1998. A comparison of encephalization between odontocete cetaceans and anthropoid primates. *Brain Behav Evol* 51:230–238.
- Marino L, Rilling JK, Lin SK, Ridgway SH. 2000. Relative volume of the cerebellum in dolphins and comparison with anthropoid primates. *Brain Behav Evol* 56:204–211.
- Marino L, Murphy TL, Gozal L, Johnson JI. 2001a. Magnetic resonance imaging and three-dimensional reconstructions of the brain of a fetal common dolphin, *Delphinus delphis*. *Anat Embryol (Berl)* 203:393–402.
- Marino L, Murphy TL, Deweerd AL, Morris JA, Fobbs AJ, Humblot N, Ridgway SH, Johnson JI. 2001b. Anatomy and three-dimensional reconstructions of the brain of the white whale (*Delphinapterus leucas*) from magnetic resonance images. *Anat Rec* 262:429–439.
- Marino L, Sudheimer KD, Murphy TL, Davis KK, Pabst DA, McLellan WA, Rilling JK, Johnson JI. 2001c. Anatomy and three-dimensional reconstructions of the brain of a bottlenose dolphin (*Tursiops truncatus*) from magnetic resonance images. *Anat Rec* 264:397–414.
- Marino L, Sudheimer K, Pabst DA, McLellan WA, Johnson JI. 2003a. Magnetic resonance images of the brain of a dwarf sperm whale (*Kogia simus*). *J Anat* 203:57–76.
- Marino L, Sudheimer K, Sarko D, Sirpenski G, Johnson JI. 2003b. Neuroanatomy of the harbor porpoise (*Phocoena phocoena*) from magnetic resonance images. *J Morphol* 257:308–347.
- Marino L, Sherwood CC, Delman BN, Tang CY, Naidich TP, Hof PR. 2004a. Neuroanatomy of the killer whale (*Orcinus orca*) from magnetic resonance images. *Anat Rec* 281:1256–1263.
- Marino L, Sudheimer K, McLellan WA, Johnson JI. 2004b. Neuroanatomical structures of the spinner dolphin (*Stenella longirostris orientalis*) brain from magnetic resonance images. *Anat Rec* 279:601–610.
- Marino L, Connor RC, Fordyce RE, Herman LM, Hof PR, Lefebvre L, Lusseau D, McCowan B, Nimchinsky EA, Pack AA, Rendell L, Reidenberg JS, Reiss D, Uhen MD, Van der Gucht E, Whitehead H. 2007. Cetaceans have complex brains for complex cognition. *PLOS Biol* 5:e139.
- McArdle CB, Richardson CJ, Nicholas DA, et al. 1987. Developmental features of the neonatal brain: MR imaging. I. Gray-white matter differentiation and myelination. *Radiology* 162:223–229.
- McKinney MA, De Guise S, Martineau D, Beland P, Lebeuf M, Letcher RJ. 2006. Organohalogen contaminants and metabolites in beluga whale (*Delphinapterus leucas*) liver from two Canadian populations. *Environ Toxicol Chem* 25:30–41.
- Montie EW, Schneider GE, Ketten DR, Marino L, Touhey KE, Hahn ME. 2007. Neuroanatomy of the subadult and fetal brain of the Atlantic white-sided dolphin (*Lagenorhynchus acutus*) from in situ magnetic resonance images. *Anat Rec* 290:1459–1479.
- Moore JK, Perazzo LM, Braun A. 1995. Time course of axonal myelination in the human brainstem auditory pathway. *Hear Res* 87:21–31.
- Morgane PJ, Jacobs MS, MacFarland WL. 1980. The anatomy of the brain of the bottlenose dolphin (*Tursiops truncatus*). Surface configurations of the telencephalon of the bottlenose dolphin with comparative anatomical observations in four other cetacean species. *Brain Res Bull* 5:1–107.
- Morgane PJ, Jacobs MS, Galaburda A. 1986. Evolutionary morphology of the dolphin brain. In: Schusterman RJ, Thomas JA, Wood FG, editors. *Dolphin cognition and behavior: a comparative approach*. Hillsdale, NJ: Lawrence Erlbaum. p 5–30.
- Mukhametov LM, Supin AY, Polyakova IG. 1977. Interhemispheric asymmetry of the electroencephalographic sleep patterns in dolphins. *Brain Res* 134:581–584.
- Oelschläger HHA, Oelschläger JS. 2002. Brain. In: Perrin WF, Würsig B, Thewissen JGM, editors. *Encyclopedia of marine mammals*. San Diego: Academic Press. p 133–158.
- O'Keefe J, Nadel L. 1978. *The hippocampus as a cognitive map*. Gloucestershire, UK: Clarendon Press.
- Pantel J, O'Leary DS, Cretsinger K, Bockholt HJ, Keefe H, Magnotta VA, Andreasen NC. 2000. A new method for the in vitro volumetric measurement of the human hippocampus with high neuroanatomical accuracy. *Hippocampus* 10:752–758.
- Ridgway SH. 1990. The central nervous system of the bottlenose dolphin. In: Leatherwood S, Reeves R, editors. *The bottlenose dolphin*. San Diego: Academic Press. p 69–97.
- Ridgway SH, Brownson RH. 1984. Relative brain sizes and cortical surface areas in odontocetes. *Acta Zool Fenn* 172:149–152.
- Rilling JK, Insel TR. 1999. The primate neocortex in comparative perspective using magnetic resonance imaging. *J Hum Evol* 37:191–223.
- Sandala GM, Sonne-Hansen C, Dietz R, Muir DCG, Valters K, Bennett ER, Born EW, Letcher RJ. 2004. Hydroxylated and methyl sulfone PCB metabolites in adipose and whole blood of polar bear (*Ursus maritimus*) from East Greenland. *Sci Total Environ* 331:125–141.
- Scholin CA, Gulland F, Doucette GJ, Benson S, Busman M, Chavez FP, Cordaro J, DeLong R, De Vogelaere A, Harvey J, Haulena M, Lefebvre K, Lipscomb T, Loscutoff S, Lowenstine LJ, Marin R III, Miller PE, McLellan WA, Moeller PD, Powell CL, Rowles T, Silvagni P, Silver M, Spraker T, Trainer V, Van Dolah FM. 2000. Mortality of sea lions along the central California coast linked to a toxic diatom bloom. *Nature* 6765:80–84.
- Sergeant DE, St. Aubin DJ, Geraci JR. 1980. Life history and Northwest Atlantic status of the Atlantic white-sided dolphin, *Lagenorhynchus acutus*. *Cetology* 37:1–12.
- Sharlin DS, Bansal R, Zoeller RT. 2006. Polychlorinated biphenyls exert selective effects on cellular composition of white matter in a manner inconsistent with thyroid hormone insufficiency. *Endocrinology* 147:846–858.
- Silvagni PA, Lowenstine LJ, Spraker T, Lipscomb TP, Gulland FMD. 2005. Pathology of domoic acid toxicity in California sea lions (*Zalophus californianus*). *Vet Pathol* 42:184–191.
- Solntseva G. 1999. The comparison of the development of the auditory and vestibular structures in toothed whales - beluga (Cetacea: Odontoceti - *Delphinapterus leucas*). *Dokl Akad Nauk* 364:714–718.
- Stephan H, Frahm H, Baron G. 1981. New and revised data on volumes of brain structures in insectivores and primates. *Folia Primatol* 25:1–29.
- Tarpley RL, Ridgway SH. 1994. Corpus callosum size in delphinid cetaceans. *Brain Behav Evol* 44:156–165.
- Thompson RK, Herman LM. 1977. Memory for lists of sounds by the bottlenose dolphin: convergence of memory processes with humans? *Science* 195:501–503.
- Viberg H, Fredriksson A, Eriksson P. 2003. Neonatal exposure to polybrominated diphenyl ether (PBDE 153) disrupts spontaneous behaviour, impairs learning and memory, and decreases hippocampal cholinergic receptors in adult mice. *Toxicol Appl Pharmacol* 192:95–106.
- Wells RS, Tornero V, Borrell A, Aguilar A, Rowles TK, Rhinehart HL, Hofmann S, Jarman WM, Hohn AA, Sweeney JC. 2005. Integrating life-history and reproductive success data to examine potential relationships with organochlorine compounds for bottlenose dolphins (*Tursiops truncatus*) in Sarasota Bay, Florida. *Sci Total Environ* 349:106–119.